NDT and E International 98 (2018) 147–154

Contents lists available at ScienceDirect

NDT and E International

journal homepage: www.elsevier.com/locate/ndteint

The use of pulse-compression thermography for detecting defects in paintings

S. Laureti [a,*], S. Sfarra [b], H. Malekmohammadi [a], P. Burrascano [a], D.A. Hutchins [c], L. Senni [a], G. Silipigni [a], X.P.V. Maldague [d], M. Ricci [e]

[a] Department of Engineering, Polo Scientifico Didattico di Terni, University of Perugia, Strada di Pentima 4, 05100, Terni, Italy
[b] Department of Industrial and Information Engineering and Economics, University of L'Aquila, Piazzale E. Pontieri 1, 67100, Loc. Monteluco di Roio, L'Aquila, AQ, Italy
[c] School of Engineering, University of Warwick, Library Road, CV4 7AL, Coventry, United Kingdom
[d] Department of Electrical and Computer Engineering, Laval University, 1065, av. de la Médecine, G1V 0A6, Québec City, QC, Canada
[e] Department of Informatics, Modeling, Electronics and Systems Engineering, University of Calabria, Via Pietro Bucci, 87036, Arcavacata, Rende CS, Italy

ARTICLE INFO

Keywords:
Thermography
Coded excitation
Pulse-compression
Paintings

ABSTRACT

Interest in the conservation of paintings grows year by year. Their periodic inspection is essential for their conservation over the time. Thermographic non-destructive inspection is one technique useful for paintings, but it is essential to be able to detect buried defects while minimising the level of thermal stimulus. This paper describes a pulse-compression infrared thermography technique whereby defect detection is optimized while minimising the rise in temperature. To accomplish this task, LED lamps driven by a coded waveform based on a linear frequency modulated chirp signal have been used on paintings on both a wooden panel and a canvas layer. These specimens contained artificially fabricated defects. Although the physical condition of each painting was different, the experimental results show that the proposed signal processing procedure is able to detect defects using a low temperature contrast.

1. Introduction

Active Thermography (AT) is a Non-Destructive Evaluation (NDE) technique widely used in different fields of research and industrials applications, as in material characterization [1], food inspection [2] and in cultural heritage diagnostic [3]. AT always relies on exciting the sample with a heating stimulus to achieve the required thermal contrast, though many different measurement schemes and post-processing algorithms can be employed [4]. For cultural heritage objects, AT is commonly implemented using Pulsed Thermography (PT), where the sample *e.g.* a bookbinding [5], bronze statue [6] or painting [7] is excited by an impulse from a flash-lamp. Additional thermal stimuli that have been reported include hot air [8], cold air [9], quartz lamps linear systems [10], heating plates [11], halogen lamps [12] and laser heating [13]. Information about defects and other structural changes are retrieved by analysing both the heating and cooling response as a function of time and location.

Although PT is relatively simple to use, care should be taken when applying a pulsed stimulus to cultural objects such as paintings. This is because abrupt variations of the sample temperature could create thermal shocks and hence damage to the sample, although these can be anticipated using numerical simulations centred on heat transfer phenomena [14,15]. In particular, colour changes (known as thermochromism) may result, where a particular pigment may react to long (or repetitive) exposures to high temperatures, leading to degradation of the perceived colour. In addition, an exposed area may drift to another shade of colour. Certain colours formed by pigments are more susceptible to this drift [16]. For example, in vivianite ($Fe_3(PO_4)_2{\cdot}8H_2O$, blue), heat-related damage can be observed at temperatures as low as 70 °C, causing colour changes in both pure vivianite [17] and oil paint layers containing it [18]. Thus, minimising the temperature variation is of primary importance. The use of low-power excitation is therefore desirable in such cases, but this leads to a significant reduction of the Signal to Noise Ratio (SNR) that could affect the effectiveness of the PT analysis.

Fortunately, techniques have been developed capable of improving the SNR of AT measurements in case of low-power sources. One approach

* Corresponding author.
E-mail addresses: stefano.laureti@unipg.it, lauretistefano@gmail.com (S. Laureti), stefano.sfarra@univaq.it (S. Sfarra), hamed.malekmohammadi@unipg.it (H. Malekmohammadi), pietro.burrascano@unipg.it (P. Burrascano), D.A.hutchins@warwick.ac.uk (D.A. Hutchins), luca.senni@unipg.it (L. Senni), giuseppe_silipigni@hotmail.com (G. Silipigni), Xavier.Maldague@gel.ulaval.ca (X.P.V. Maldague), m.ricci@dimes.unical.it (M. Ricci).

https://doi.org/10.1016/j.ndteint.2018.05.003
Received 16 February 2018; Received in revised form 25 April 2018; Accepted 10 May 2018

is Lock-in Thermography (LT), where the heating stimulus is modulated at a specific frequency [19]. The acquired thermograms are then processed in the frequency domain, thus obtaining phase and magnitude images of the investigated item at that frequency [20]. LT is widely adopted as it provides a significant gain of SNR. However, the depth of penetration is set by the modulation frequency, and the amount of information retrieved is lower than that from PT, which excites a greater measurement bandwidth [21]. Therefore, efforts have been made to combine the advantages of both schemes, leading for example to Pulse Phase Thermography [22], and the more complex Multi-Frequency Lock-in Thermography [23].

Another possible approach is to exploit the positive features of pulse-compression techniques [24]. The application of coded excitation signals and pulse-compression for studying thermal phenomena was pioneered by several rearch groups led by Mandelis [25–27] and Mulaveesala [28–30]. Subsequently, various PuCT procedures have been proposed [31–33]. In fact, the Pulse Compression (PuC) algorithm outputs an accurate impulse response estimate that is very similar to that obtainable from PT, even when low-power sources are used. The modulated heating stimulus is in the form of a coded excitation, where the bandwidth B and the duration T of the signal are uncorrelated. Hence, the frequency content of the coded signal can be tailored to suit the investigation of a given sample, while T can be increased almost arbitrarily to achieve the desired SNR [34–37]. These properties can be usefully applied to inspect paintings, using low-power heating sources to keep surface temperatures relatively low. Moreover, the use of coded excitations and PuC allows both frequency and time domain analyses to be performed. A frequency domain analysis can be carried out directly on the raw acquired data; the time domain analysis can be executed after the application of the PuC algorithm. It is worth noting that the use of pseudo-random modulated heating stimulus has been used in infrared thermography [25], and recently applied in AT for cultural heritage diagnostic by Candoré et al. [38]. However, here the thermal impulse response was estimated using an Auto Regressive Moving Average algorithm (ARMA) to model the process. In PuCT, the thermal impulse response is estimated by applying a deterministic procedure based on application of a matched filter. In addition, in Ref. [38] the thermal source consisted of halogen lamps driven by a pseudo-random code while in the present paper the heating stimulus is realized with LEDs driven by a chirp signal.

Here we extend the above by investigating the use of PuCT for the NDE of paintings. PuCT has been performed on two different specimens, representing two painting types: one being a painted wooden panel [39,40], the other a painting on canvas [41,42], both containing artificial defects. It should be noted that each of these samples aims to mimic the painting technique of a specific artistic period. In particular, the panel painting was constructed following the Cennino Cennini's rules [43], thus mimicking a painting technique often used during the XV century. The painting on canvas is close to contemporary art where acrylic-based paint is used [44]. Therefore, the artistic period to which they refer is completely different. For the current setup, the heating source consisted of eight LED chips which provided an overall power of 110 W, low enough to avoid overheating of the sample. The coded waveform used for this work was chosen carefully so as to minimise damage to the paintings. It was a linear frequency-modulated chirp signal, a sinusoidal signal whose frequency varies linearly as time elapses [45,46], where the instantaneous chirp amplitude varies smoothly with time. Thus, the combined use of PuC and a well-designed linear chirp was able to damp any thermal shock to the paintings (especially when compared to PT), while minimising increases in the sample temperature.

2. Description of the samples

2.1. Painting on canvas

Here, a linen canvas was used as support, and after a preliminary treatment (sizing), the canvas was fixed onto a wooden frame. An outline charcoal crayon sketch was drawn on the canvas (Fig. 1(a)). Two Mylar defects were then placed between the size and the ground layers, see Fig. 1(b) and (d). Defect A (4.5 × 1 cm) consisted of two superimposed Mylar layers, and defect B (4 × 1 cm) was formed from one layer. Acrylic paint and varnish layers were then applied over the defects and the canvas was both embroidered (see the arrows in Fig. 1(c)), and other repairs simulated using a crochet-hook. The final appearance of the painting is shown in Fig. 1(e).

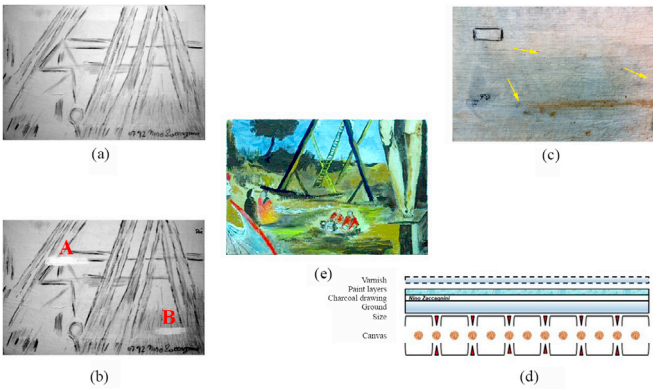

Fig. 1. Painting on canvas: (a) the preparatory drawing, (b) defects A, B, (c) back view with embroideries, (d) the layers constituting the sample, and (e) front view of the final sample.

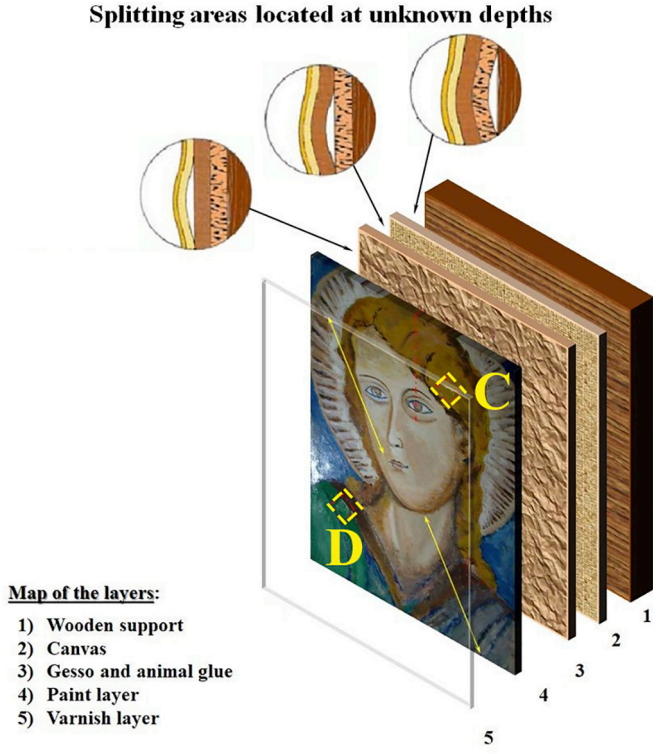

Fig. 2. Panel painting: on-plane position of the fabricated defects and sequence of the layers.

2.2. Wooden panel painting

The panel painting, based on a poplar wood substrate with dimensions (20 × 25 × 2 cm), is shown in Fig. 2(a) along with the positions of the defects (labelled C-D). Poplar was frequently used for the fabrication of panel paintings in the Italian schools [43]. Splitting areas were simulated by inserting a thin sponge covered with Mylar (defect C) and a

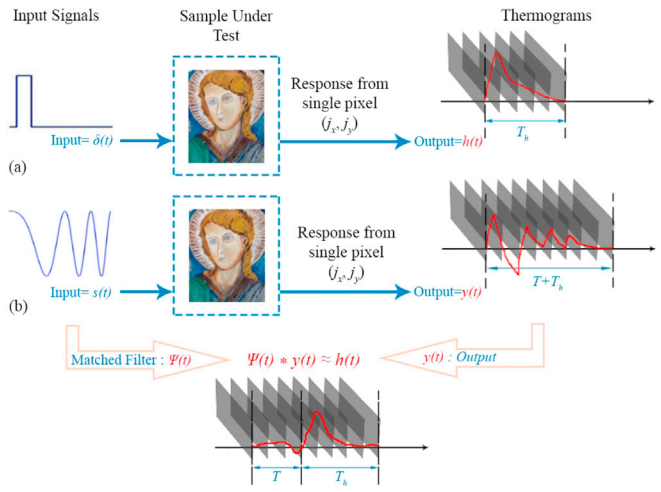

Fig. 3. Comparison between (a) pulsed thermography (PT) and (b) Pulse-compression thermography (PuCT) procedures.

Mylar sheet (defect D) at different depths beneath the paint layer. The gilding layer was not applied in this case, while oil colours where used to finalize the sample. Other satellite defects were also possibly present due to the nature of poplar wood, which is normally soft, weak, fine-grained, diffuse-porous, with small pores in term of size [47].

3. Theoretical background

Heat transfer is a very complex phenomenon for which many references can be found in literature. The reader is referred to [48–50] for a detailed mathematical description of the heat transfer within a body when AT is performed, particularly for the case of PuCT [28–33]. The following subsections are aimed at showing the basic mathematical theory at the heart of PuCT, its pros and cons with respect to standard pulsed excitation, and how to correctly apply this technique for NDE. Moreover, the main features of the employed linear chirp signal are also shown.

3.1. Pulse-compression basic theory

PuC is a measurement technique employed to estimate the impulse response $h(t)$ of Linear Time Invariant (LTI) systems in poor SNR conditions. In standard PT, flash lamps are usually exploited to heat the sample within a time significantly shorter than the typical cooling time of the sample itself. Thus, the heating stimulus exciting the LTI system can be modelled as a Dirac's Delta function $\delta(t)$ so that the corresponding impulse response $h(j_x, j_y, t)$ is directly retrieved as the pixel temperature/emissivity time trend (see Fig. 3(a)). Useful information about the sample are obtained by analysing both the heating and the cooling of the $\{h(j_x, j_y, t)\}$ within a chosen range of interest T_h. PuCT requires further processing steps to be performed, as it relies on the existence of two signals $\{s(t), \Psi(t)\}$ such that their convolution $\tilde{\delta}(t)$ approximates the Dirac's Delta Function $\delta(t)$:

$$s(t)*\Psi(t) = \tilde{\delta}(t) \approx \delta(t) \tag{1}$$

where $*$ denotes a convolution, $s(t)$ is the coded excitation of duration T and bandwidth B, and $\Psi(t)$ is the so-called matched filter. If Eq. (1) holds, an estimate $\tilde{h}(j_x, j_y, t)$ of the $h(j_x, j_y, t)$ is obtained by exciting the LTI system with $s(t)$ and then by convolving the acquired system output $y(j_x, j_y, t)$ with $\Psi(t)$, see Fig. 3(b). This is demonstrated in Eq. (2) for a single pixel of the acquired image, where also the presence of an Additive-White-Gaussian-Noise (AWGN) as the $e(t)$ term, uncorrelated to $\Psi(t)$), is considered.

In PT the excitation is considered instantaneous and the sample impulse thermal response is measured for a time T_h, which is the impulse response time duration, *i.e.* the time necessary for the diffusion of the heat. In PuCT, the sample is excited with a coded excitation of duration T and thermograms are collected for an overall time duration of $T + T_h$. After the application of the PuC algorithm, an estimated impulse thermal response of duration T_h is retrieved.

$$\tilde{h}(t) = y(t)*\Psi(t) = h(t)*\underbrace{s(t)*\Psi(t)}_{=\tilde{\delta}(t)} + e(t)*\Psi(t) = h(t)*\tilde{\delta}(t) + \tilde{e}(t)$$
$$\approx h(t) + \tilde{e}(t) \tag{2}$$

The use of PuC instead of pulsed excitation results in an estimate $\tilde{h}(t)$ of the $h(t)$ having an increased SNR. The SNR gain is proportional to the $T \cdot B$ product, *i.e.* it can be enhanced almost arbitrarily by increasing either the time duration or the bandwidth of the coded waveform. Under the hypothesis of AWGN noise, the use of a matched filter defined as $\Psi(t) = s(-t)$ maximizes the SNR for a given setup [51]. Drawbacks of the use of PuC arise from the practically-limited T and B values that lead to an approximated reconstruction of the real impulse response $h(t)$ [52]. Only an approximation $\tilde{h}(j_x, j_y, t)$ can be retrieved after PuC, the quality of this approximation being dependent on the level of sidelobes associated with $\tilde{\delta}(t)$. Therefore, it is important to reduce the magnitude of the sidelobes, as they can reduce the defect detection capability. Many studies can be found showing different approaches for optimizing the design of both the coded waveform and the matched filter, either for decreasing their magnitude or for maximizing the SNR gain. Although an exhaustive investigation lies beyond the scope of the present work, it has been observed that replacing the standard matched filter with a Wiener filter helps on minimising sidelobe amplitudes [51–54]. Finally, the quality of reconstructing $\tilde{\delta}(t)$ depends strictly on the correct implementation of the convolution procedure. The reader is referred to [31–37,55–61] for further details.

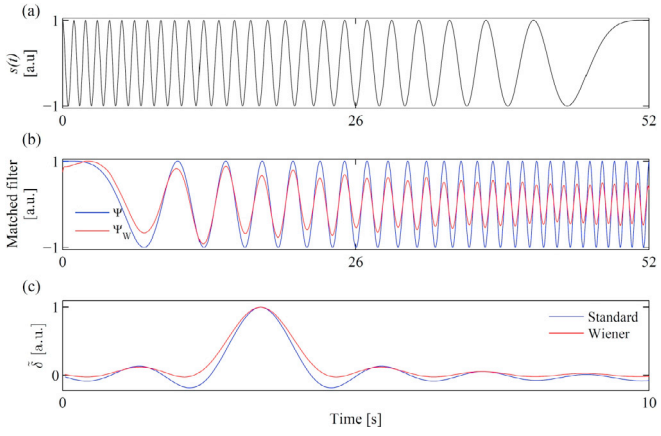

Fig. 4. (a) Employed chirp signal time handling; (b) comparison between standard matched filter $\Psi(t)$ (blue) and proposes Wiener filter $\Psi_W(t)$ (red) time handling; (c) comparison between $\tilde{\delta}(t)$ obtained by using either $\Psi(t)$ (blue) or $\Psi_W(t)$ (red).

3.2. Linear chirp signal and optimized Wiener filter

A linear chirp signal is a frequency modulated signal whose instantaneous frequency varies linearly within a chosen range. A general mathematical definition of a chirp is given here:

$$s(t) = \cos(\varphi(t)) \tag{3}$$

with $\varphi(t)$ the instantaneous signal phase. The design of a chirp strictly depends from the definition of the instantaneous frequency $f_{ist}(t)$:

$$f_{ist}(t) = \frac{1}{2\pi}\frac{d\varphi(t)}{dt} \tag{4}$$

For a linear chirp signal, the phase is a quadratic function $\varphi(t) = f_0 t + \frac{B}{2T}t^2$, leading to an expression for $f_{ist}(t)$ that is a linear function of time:

$$f_{ist}(t) = f_0 + \frac{B}{T}t, \tag{5}$$

where B is the bandwidth $B = f_1 - f_0$, being the difference between the initial and the final value of the instantaneous chirp frequency. Note that if $f_1 > f_0$ and $B > 0$, $f_{ist}(t)$ increases as time elapses and the chirp is called "up" linear chirp; otherwise if $f_1 < f_0$, $f_{ist}(t)$ decreases as time elapses and the chirp is a "down" linear chirp. Although an "up" linear chirp could also be employed, hereinafter a "down" chirp signal is considered, spanning the frequency range within $f_1 = 0$ Hz and $f_0 = 1$ Hz for an overall duration of $T = 52$ s, as depicted in Fig. 4(a). Please note that the selected frequency range has been chosen so as to guarantee sufficiently-large thermal diffusion lengths, thus allowing an increased penetration within the inspected sample; in addition, the $T \cdot B$ product is high enough to provide a sufficient SNR value [35,58,62,63]. Finally, the extended duration of the coded signal, together with its smooth instantaneous amplitude transition (Fig. 4(a)), helps to avoid any thermal shock.

As mentioned above, Wiener Filtering suppresses the magnitude of $\tilde{\delta}(t)$ sidelobes by up to 30 dB with respect to what is achievable by employing a matched filter $\Psi(t) = s(-t)$ [26]. Applying a Wiener filter simply consists of substituting $\Psi(t)$ with a new matched filter $\Psi_W(t)$, defined as in Eq. (6):

$$\Psi_W(t) = IFFT\left(\frac{\Psi(f)}{|\Psi(f)|^2 + a + b\cdot|f|}\right) = IFFT\left(\frac{s^*(f)}{|s(f)|^2 + a + b\cdot|f|}\right), \tag{6}$$

where IFFT stands for Inverse Fast Fourier Transform operator, a and b are two regularization parameters, the former regulating the filter effect over the entire bandwidth and the latter penalizing the high frequencies. The values used for the regularization parameters were $a = b = 0.1$. Eq. (6) shows that $\Psi_W(t)$ has the same phase profile of the $\Psi(t)$, but with a modified spectrum amplitude. Fig. 4(b) depicts both the standard $\Psi(t)$ and the optimized $\Psi_W(t)$, whilst a comparison between the obtained $\tilde{\delta}(t)$ with the said matched filters is shown in Fig. 4(c). Fig. 4(c) shows that the use of Wiener filter $\Psi_W(t)$ leaves the main lobe amplitude almost unaltered with respect to use the standard $\Psi(t)$, while providing a significant sidelobe reduction. Therefore, the resulting $\tilde{\delta}(t)$ quality is improved, leading to a better $\tilde{h}(t)$ estimate.

4. The use of pulse compression in active thermography

From the above, it will be apparent that the quality of the estimated $\tilde{h}(t)$ of the real impulse response $h(t)$ obtained by performing PuC depends not only on the correct choice of the coded signal parameters and the related matched filter (both discussed above), but also on the correct implementation of the convolution procedure, where issues will arise from the difficulty in realizing a bipolar heating source. Therefore, an offset must be applied to the chirp signal $s(t)$ so as to create the correct heating source (which must be monopolar). It thus follows that the real employed excitation signal $s_{TR}(t) = s(t) + s_{SQ}(t)$ is the superposition of a chirp signal $s(t)$ and a square pulse $s_{SQ}(t) = C\{\vartheta(t) - \vartheta(t-T)\}$ where $\vartheta(t)$ is the Heaviside step function. Thus, the true acquired output signal (Eq. (7)) will be:

$$y_{TR}(t) = h(t)*s(t) + h(t)*s_{SQ}(t) + e(t) = y(t) + y_{SQ}(t) + e(t) \tag{7}$$

Consequently, the contribution of $y_{SQ}(t)$ from $y(t)$ must be removed before finalizing the PuC algorithm via convolution with the matched filter. For clarity, this requirement can be realized by comparing Eq. (7) with Eq. (2).

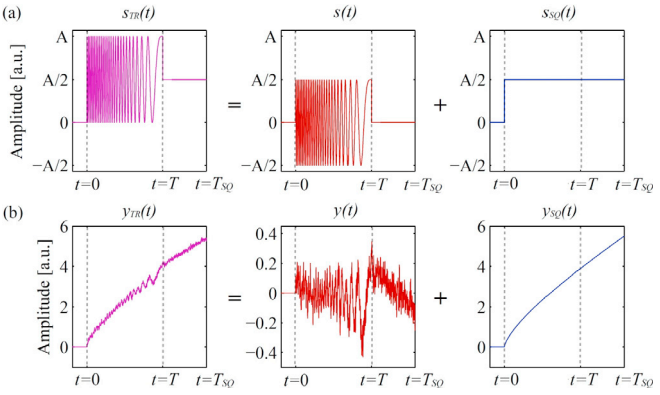

Fig. 5. (a) True excitation $s_{TR}(t)$and (b) true output $y_{TR}(t)$ signals. $y(t)$ is retrieved after performing a non-linear fitting procedure to remove completely the $y_{SQ}(t)$ contribution.

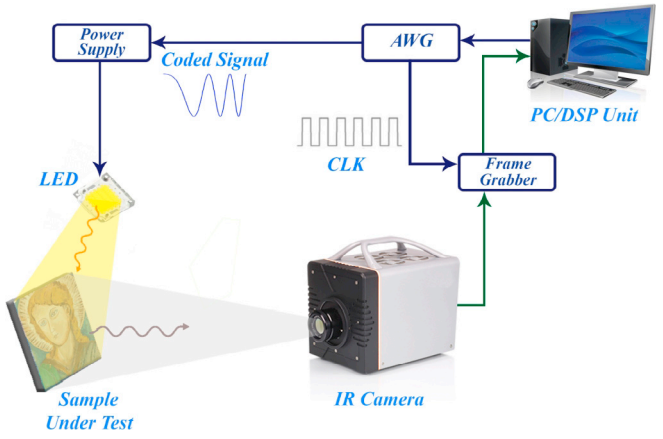

Fig. 6. The experimental setup. The Arbitrary Waveform Generator (AWG) and Frame Grabber were connected to a PC. The AWG board provided both the wanted linear chirp excitation and a reference clock signal (CLK) for triggering the IR camera acquisition. The coded signal was input into a TDK Lambda GEN 750 W power supply that fed eight LED chips placed at about 30 cm from the sample under test.

Recently, Silipigni et al. [33] proposed a procedure for proper implementing PuC in AT based on extending the $s_{SQ}(t)$ contribution for some time after T. It has been shown that this helps to design an optimized non-linear fitting algorithm, capable of correctly removing the contribution $y_{SQ}(t)$ from $y(t)$.

In summary, the PuCT procedure should use the following steps:

1) Excite the sample with a chirped heating stimulus of time duration T and with an additional $s_{SQ}(t)$ contribution for $T_{SQ} = T + T_h > T$. In the present work, $T_{SQ} = 82$ s, $T = 52$ s and $T_h = 30$ s. Thus, the sample is kept heated for 30 s after the end of the coded stimulus.
2) Acquire thermograms for an overall time interval T_{SQ}.
3) Remove the $y_{SQ}(t)$ contribution from each pixel of the acquired thermographic sequence, thus obtaining $y(t)$.
4) Perform a pixel-by-pixel convolution of each $y(t)$ with the optimized $\Psi_W(t)$, *i.e.* retrieving the $\tilde{h}(j_x, j_y, t)$.

The true output signals are reported in Fig. 5, where the role of the step-heating is also highlighted.

5. Experimental setup

A sketch of the experimental setup is shown in Fig. 6.

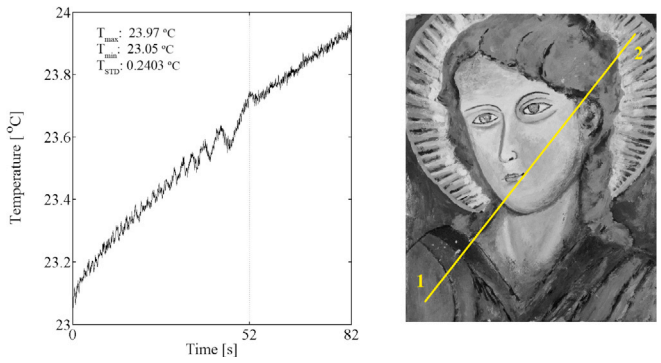

Fig. 7. Averaged temperature time handling of a line of pixels (1–2) crossing the panel painting surface while subject to the employed heating stimulus. Maximum (T_{max}), minimum (T_{min}) and standard deviation (T_{STD}) values are reported inside the plot.

A National Instrument PCI-6711 Arbitrary Waveform Generator (AWG) board and a National Instrument 1433 Camera Link Frame Grabber were connected to a PC, and an ad hoc developed virtual instrument in LabVIEW™ managed the signal generation/acquisition. The AWG board provided both the wanted linear chirp excitation and a reference clock signal (CLK) for triggering the IR camera acquisition, which was a Xenics Onca-MWIR-InSb IR camera. The coded signal was input into a TDK Lambda GEN 750 W power supply that fed eight LED chips placed at about 30 cm from the SUT. The LED chips are capable of providing a maximum overall power of 400 W but the total employed power was reduced to 110 W to avoid overheating of the sample. In addition, Xeneth™ software provided by the camera manufacturer was used for estimating the temperature increment at the sample caused by a particular chirp-modulated heating stimulus. The thermograms were acquired at 40 FPS.

6. Results

As already pointed out, it is important to keep the painting temperature increase as low as possible during the inspection. Preliminary results show that a temperature increment of ~1 °C occurred at the sample surface. This is illustrated in Fig. 7, where the temperature profile averaged over a line of pixels (1–2) crossing the panel painting surface is plotted as the time elapsed.

Figs. 8 and 9 show the effect of the overall PuC procedure on defect detection and resolution by reporting a graphical comparison between thermograms collected during both the application of the chirp excitation (Figs. 8(a) and 9(a)) and after PuC (Figs. 8(b) and 9(b)). An improvement in the SNR of the image is clearly visible after PuC with respect to the acquired raw data. Also, areas containing defects appeared as bright pixels areas on the sliced thermogram sequences after PuC (Figs. 8(b) and 9(b)).

Fig. 10 depicts two frames selected for both the canvas (Fig. 10(a)) and the panel sample (Fig. 10(b)) in which the defected areas detected are highlighted by yellow markers. These frames have been selected after a qualitative analysis of the recovered thermograms after PuC, *i.e.* by selecting the frames at which the defected areas appear to be clearly visible. The subsurface embroideries realized in the canvas layer of the painting on canvas are also detectable. They are indicated by arrows in Fig. 10(a).

The use of a coded heating stimulus provides the possibility of performing a simultaneous frequency and time analysis directly on the raw data (see Fig. 8(a) or Fig. 9(a)). In order to have a comparison of the results obtained with PuCT and another AT technique, a LT experiment was conducted. Since the selection of the optimal modulation frequency in LT is essential, a FFT analysis on the raw PuCT data was performed to

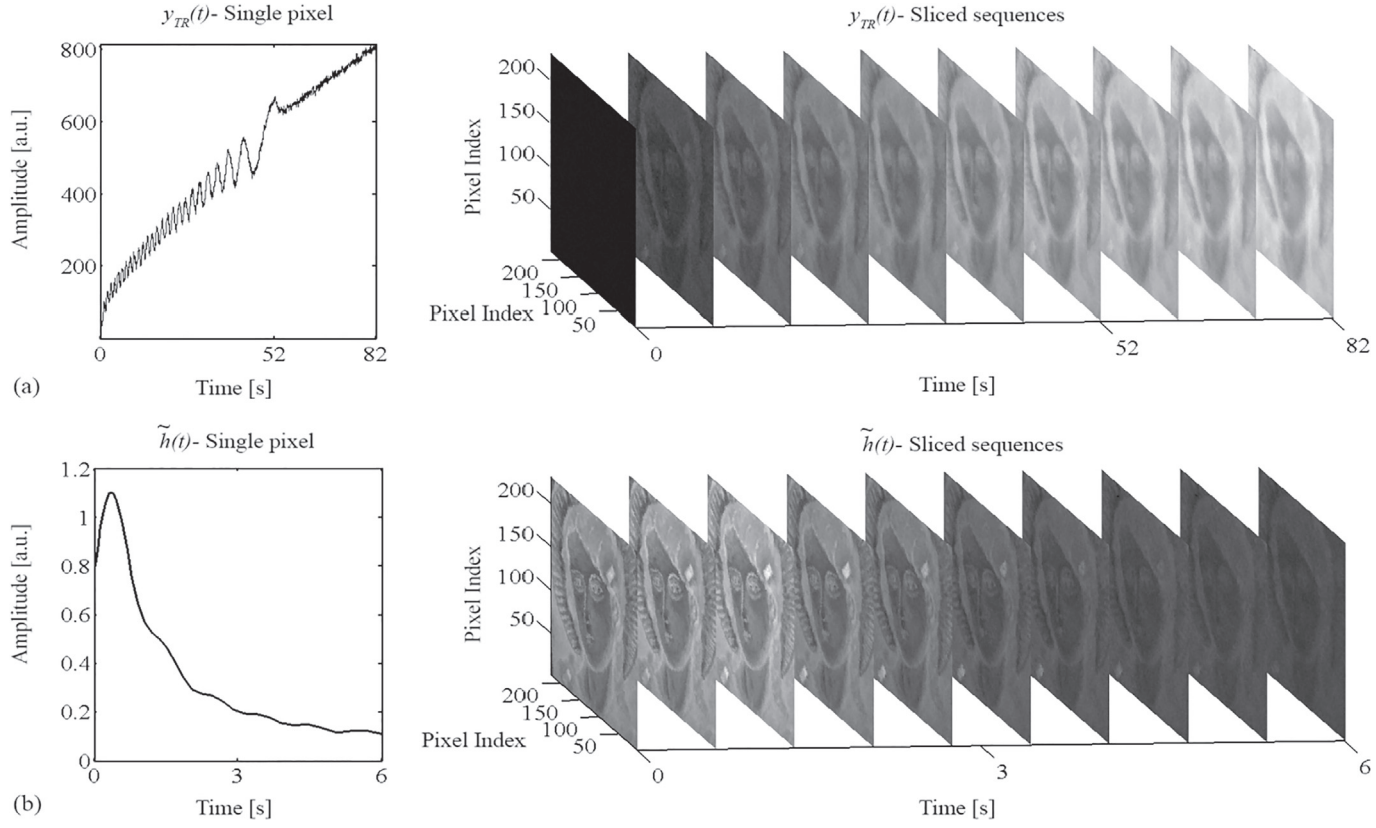

Fig. 8. (a) Comparison between thermograms collected at different times during the application of the chirp excitation; (b) thermograms retrieved after pulse compression, panel painting.

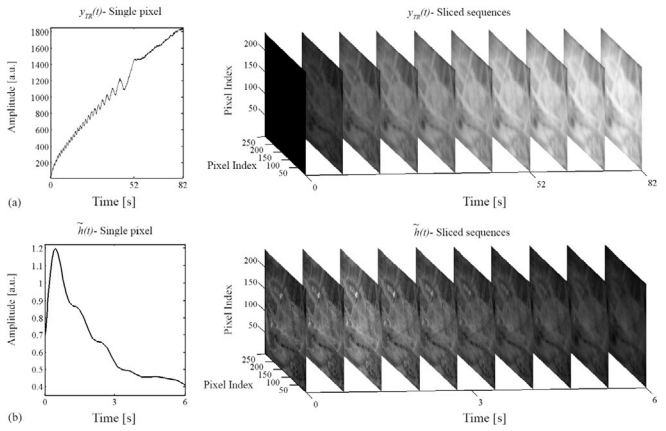

Fig. 9. (a) Comparison between thermograms collected at different times during the application of the chirp excitation; (b) thermograms retrieved after pulse compression, canvas painting.

qualitatively select the best frame and its corresponding frequency for each SUT. In particular, it has been found that the best frame is obtained at around 0.15 Hz for canvas and around 0.19 Hz for the panel. Therefore, LT was carried out using a sinusoid modulation at these frequencies using the same 110 W LED setup for 82 s, so as to be consistent with T_{SQ}, see Section IV. Results obtained from FFT analysis (magnitude) on both the acquired raw PuCT data (Fig. 11) and LT results (Fig. 12) on both samples can be compared, where differences are apparent, which are discussed below.

Embroideries are the most difficult defects to be detected due to their tiny dimension and the similarity to the surrounding canvas texture. Fig. 13 shows the LT phase image of the canvas sample.

7. Discussion

The results obtained using the proposed PuCT approach are qualitatively comparable to the ones obtained by LT technique. This can be seen if Fig. 10(a) and (b) are compared with Fig. 12(a) and (b) respectively. In addition, it should be noted that the modulation frequency value used for LT should have been known *a priori* for the best result, whilst it has been chosen here after an FFT analysis of the PuCT raw data. The quality of the phase image obtained with LT on the canvas (Fig. 13) is qualitatively comparable with the one obtained with PuCT on the same sample in time domain (Fig. 10(a)). Indeed, in both cases all the defects in the canvas are clearly visible. Finally, the thermograms obtained from PuCT in Figs. 8(b) and 9(b) shows that a time analysis of the sample investigated features can be performed, as is also possible in PT.

8. Conclusions

In this work, the PuCT technique was applied on paintings with the aim to detect subsurface defects. In addition, the well-known LT technique was used for comparative purposes. The PuCT technique was able to detect splitting areas located beneath two different paint layers that were applied on panel and canvas supports, respectively. Strategies adopted were able to improve the performance of the pulse-compression active thermography, and the experimental results demonstrated the

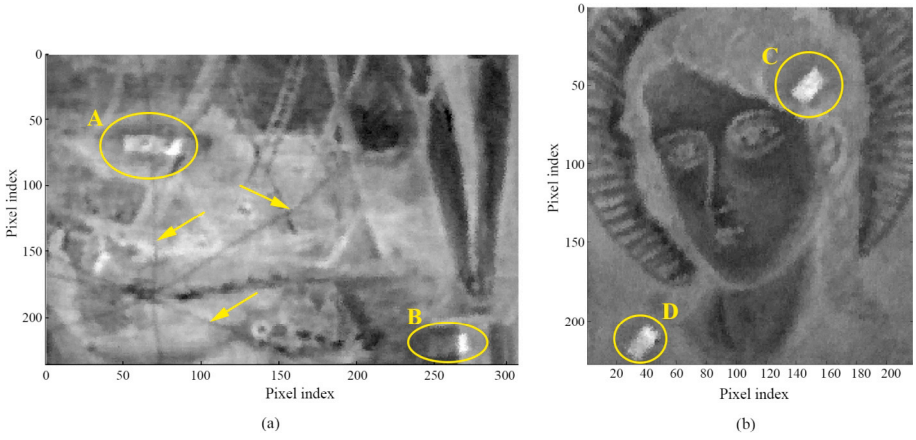

Fig. 10. Selected best frames after PuC for the (a) canvas and (b) panel painting. Yellow markers show defect A-B-C-D and embroideries.

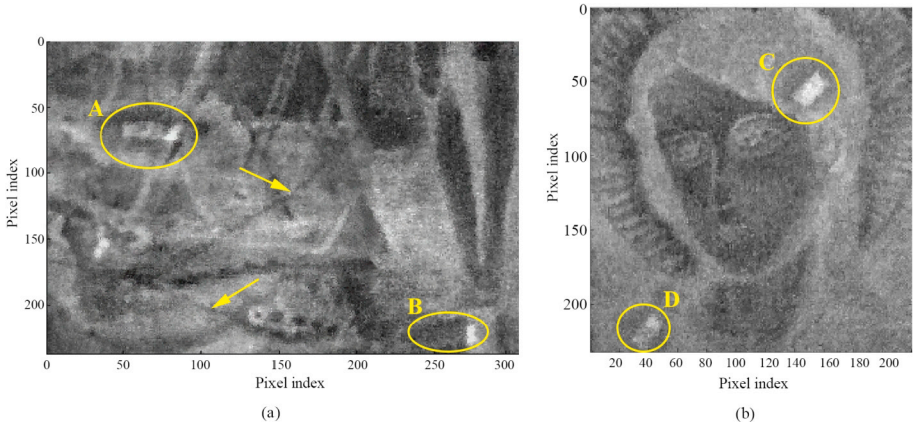

Fig. 11. Selected best frames after FFT (magnitude) for the (a) canvas at 0.15 Hz and (b) panel painting at 0.19 Hz.

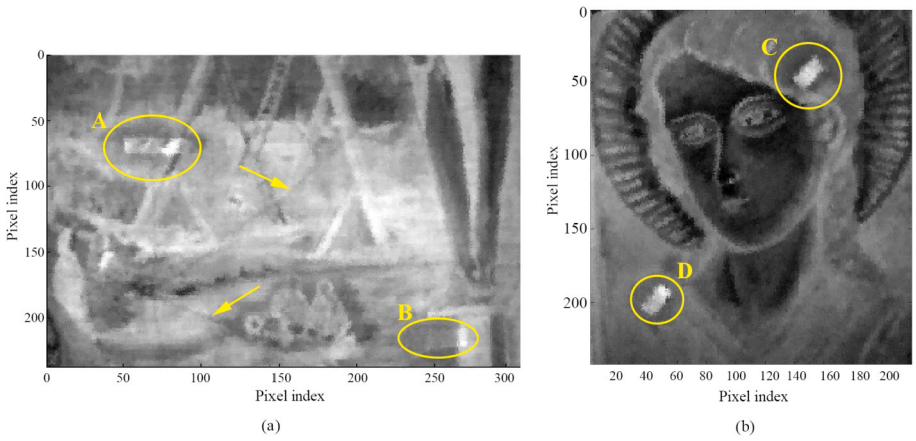

Fig. 12. Selected best frames (magnitude) after LT for the (a) canvas at 0.15 Hz and (b) panel painting at 0.19 Hz.

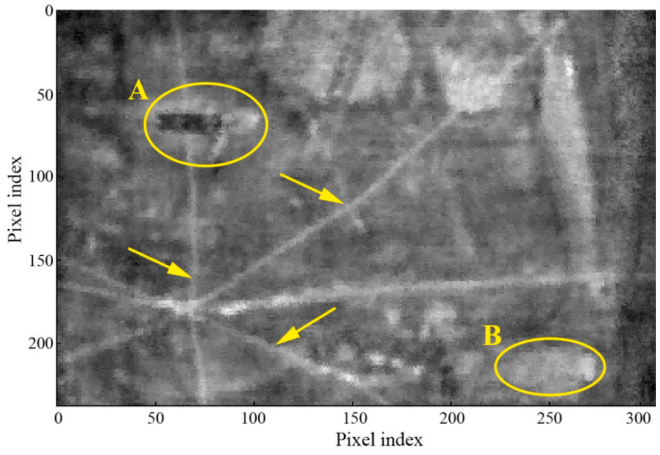

Fig. 13. Phase image after LT for the canvas painting.

gain provided by such procedures. The thermal impulse response of the inspected samples was reconstructed using an improved SNR and enhanced fidelity. A very low temperature difference causing a reasonable thermal stress on the upper layers was taken into account during thermographic inspections. Also, the type of penetration of the thermal waves appears sufficient to detect thin defects, such as crochet-work stitched areas created in the canvas. Future work intends to investigate coded excitations with an arbitrary power spectrum, intended to further increase the SNR of the deepest defects and reducing sidelobe levels.

Acknowledgments

The authors would like to thank Mr. Nino Zaccagnini (University of L'Aquila, Italy) who constructed the samples used in this work. Dr. Stefano Sfarra collaborated to the achievement of the canvas painting. This research work has been partially supported from the European Union's Horizon 2020 research and innovation programme under the Marie Skłodowska-Curie grant agreement No 722134 – NDTonAIR.

References

[1] Meola C, Carlomagno GM, Giorleo L. The use of infrared thermography for materials characterization. J Mater Process Technol 2004;155:1132–7.
[2] Weschenfelder AV, Maldague X, Rocha LM, Schaefer AL, Saucier L, Faucitano L. The use of infra-red thermography for pork quality prediction. Meat Sci 2014;96:120–5.
[3] Sfarra S, Ibarra-Castanedo C, Paoletti D, Maldague X. Infrared vision inspection of cultural heritage objects from the city of l'Aquila, Italy and its surroundings. Mater Eval 2013;71(5).
[4] Ibarra-Castanedo C, Bendada A, Maldague X. Image and signal processing techniques in pulsed thermography. GESTS Int Trans Comput Sci Eng 2005;22(1):89–100.
[5] Mercuri F, Cicero C, Orazi N, Paoloni S, Marinelli M, Zammit U. Infrared thermography applied to the study of cultural heritage. Int J Thermophys 2015;36(5–6):1189–94.
[6] Mercuri F, Paoloni S, Orazi N, Cicero C, Zammit U. Pulsed infrared thermography applied to quantitative characterization of the structure and the casting faults of the Capitoline She Wolf. Appl Phys Mater Sci Process 2017;123(5):327.
[7] Gavrilov D, Maeva E, Grube O, Vodyanoy I, Maev R. Experimental comparative study of the applicability of infrared techniques for non-destructive evaluation of paintings. J Am Inst Conserv 2013;52(1):48–60.
[8] Di Tuccio MC, Ludwig N, Gargano M, Bernardi A. Thermographic inspection of cracks in the mixed materials statue: ratto delle Sabine. Herit Sci 2015;3(1):10.
[9] Ibarra-Castanedo C, Sfarra S, Ambrosini D, Paoletti D, Bendada A, Maldague X. Diagnostics of panel paintings using holographic interferometry and pulsed thermography. Quant InfraRed Thermogr J 2010;7(1):85–114.
[10] Carlomagno GM, Meola C. Comparison between thermographic techniques for frescoes NDT. NDT&E Int 2002;35(8):559–65.
[11] Bendada A, Sfarra S, Ibarra-Castanedo C, Akhloufi M, Caumes JP, Pradere C, Batsale J, Maldague X. Subsurface imaging for panel paintings inspection: a comparative study of the ultraviolet, the visible, the Infrared and the terahertz spectra. Opto-Electron Rev 2015;23(1):90–101.
[12] Bodnar JL, Nicolas JL, Candoré JC, Detalle V. Non-destructive testing by infrared thermography under random excitation and ARMA analysis. Int J Thermophys 2012;33(10–11):2011–5.
[13] Mezghani S, Perrin E, Vrabie V, Bodnar JL, Marthe J, Cauwe B. Evaluation of paint coating thickness variations based on pulsed Infrared thermography laser technique. Infrared Phys Technol 2016;76:393–401.
[14] Theodorakeas P, Avdelidis NP, Cheilakou E, Koui M. Quantitative analysis of plastered mosaics by means of active infrared thermography. Construct Build Mater 2014;73:417–25.
[15] Sfarra S, Ibarra-Castanedo C, Theodorakeas P, Avdelidis NP, Perilli S, Zhang H, Nardi I, Koui M, Maldague X. Evaluation of the state of conservation of mosaics: simulations and thermographic signal processing. Int J Therm Sci 2017;117:287–315.
[16] Coccato A, Moens L, Vandenabeele P. On the stability of mediaeval inorganic pigments: a literature review of the effect of climate, material selection, biological activity, analysis and conservation treatments. Herit Sci 2017;5(1):12.
[17] Frost RL, Weier ML, Martens W, Kloprogge JT, Ding Z. Dehydration of synthetic and natural vivianite. Thermochim Acta 2003;401(2):121–30.
[18] Čermáková Z, Švarcová S, Hradilová J, Bezdička P, Lančok A, Vašutová V, Blažek J, Hradil D. Temperature-related degradation and colour changes of historic paintings containing vivianite. Spectrochim Acta Part A Mol Biomol Spectrosc 2015;140:101–10.
[19] Carlomagno GM, Berardi PG. Unsteady thermotopography in non-destructive testing. In: Proc 3rd biannu exch (IRIE '76)vol. 24; 1976. p. 26.
[20] Kordatos EZ, Exarchos DA, Stavrakos C, Moropoulou A, Matikas TE. Infrared thermographic inspection of murals and characterization of degradation in historic monuments. Construct Build Mater 2013;48:1261–5.
[21] Maldague X. Theory and practice of infrared thermography for nondestructive testing. Wiley series in microwave and optical engineering. Wiley; 2001.
[22] Maldague X, Marinetti S. Pulse phase infrared thermography. J Appl Phys 1996;79(5):2694–8.
[23] Beuve S, Qin Z, Roger JP, Holé S, Boué C. Open cracks depth sizing by multi-frequency laser stimulated lock-in thermography combined with image processing. Sensor Actuator Phys 2016;247:494–503.
[24] Klauder JR, Price AC, Darlington S, Albersheim WJ. The theory and design of chirp radars. Bell Labs Tech J 1960;39(4):745–808.
[25] Mandelis A. Time-delay-domain and pseudorandom-noise photoacoustic and photothermal wave processes: a review of the state of the art. In: IEEE transactions on ultrasonics, ferroelectrics, and frequency controlvol. 33; 1986. p. 590–614. 5.

[26] Mandelis A. Frequency modulated (FM) time delay-domain thermal wave techniques, instrumentation and detection: a review of the emerging state of the art in QNDE applications. In: Review of progress in quantitative nondestructive evaluation. Boston, MA: Springer; 1987. p. 799–806.
[27] Peralta SB, Chen ZH, Mandelis A. Simultaneous measurement of thermal diffusivity, thermal conductivity and specific heat by impulse-response photopyroelectric spectrometry. Appl Phys A 1991;52(5):289–94.
[28] Tuli S, Mulaveesala R. Defect detection by pulse compression in frequency modulated thermal wave imaging. Quant Infrared Thermogr J 2005;2(1):41–54.
[29] Mulaveesala R, Tuli S. Digitized frequency modulated thermal wave imaging for nondestructive testing. Mater Eval 2005;63:10.
[30] Tabatabaei N, Mandelis A. Thermal-wave radar: a novel subsurface imaging modality with extended depth-resolution dynamic range. Rev Sci Instrum 2009; 80(3). 034902.
[31] Mulaveesala R, Ghali VS. Coded excitation for infrared non-destructive testing of carbon fiber reinforced plastics. Rev Sci Instrum 2011;82(5). 054902.
[32] Gong J, Liu J, Qin L, Wang Y. Investigation of carbon fiber reinforced polymer (CFRP) sheet with subsurface defects inspection using thermal-wave radar imaging (TWRI) based on the multi-transform technique. NDT E Int 2014;62:130–6.
[33] Silipigni G, Burrascano P, Hutchins DA, Laureti S, Petrucci R, Senni L, Torre L, Ricci M. Optimization of the pulse compression technique applied to the infrared thermography nondestructive evaluation. NDT&E Int 2017;87:100–10.
[34] Ricci M, Callegari S, Caporale S, Monticelli M, Battaglini L, Eroli M, Senni L, Rovatti R, Setti G, Burrascano P. Exploiting Non-Linear Chirp and sparse deconvolution to enhance the performance of pulse-compression ultrasonic NDT. In: IEEE int ultrason symp IUS; 2012. p. 1489–92.
[35] Hutchins D, Burrascano P, Davis L, Laureti S, Ricci M. Coded waveforms for optimised air-coupled ultrasonic nondestructive evaluation. Ultrasonics 2014; 54(7):1745–59.
[36] Mohamed I, Hutchins D, Davis L, Laureti S, Ricci M. Ultrasonic NDE of thick polyurethane flexible riser stiffener material. Nondestr Test Eval 2017;32(4): 343–62.
[37] Laureti S, Ricci M, Mohamed MNIB, Senni L, Davis LAJ, Hutchins DA. Detection of rebars in concrete using advanced ultrasonic pulse compression techniques. Ultrasonics April 2018;85:31–8. doi.org/10.1016/j.ultras.2017.12.010.
[38] Candoré JC, Bodnar JL, Detalle V, Grossel P. Non-destructive testing of works of art by stimulated infrared thermography. Eur Phys J Appl Phys 2012;57(2):21002.
[39] Yao Y, Sfarra S, Lagüela S, Ibarra-Castanedo C, Wu JY, Maldague XPV, Ambrosini D. Active thermography testing and data analysis for the state of conservation of panel paintings. Int J Therm Sci 2018;126:143–51.
[40] Sfarra S, Theodorakeas P, Ibarra-Castanedo C, Avdelidis NP, Paoletti A, Paoletti D, Hrissagis K, Bendada A, Koui M, Maldague X. Evaluation of defects in panel paintings using infrared, optical and ultrasonic techniques. Insight Non-Destr Test. Cond Monit 2012;54(1):21–7.
[41] Sfarra S, Ibarra-Castanedo C, Ambrosini D, Paoletti D, Bendada A, Maldague X. Discovering the defects in paintings using non-destructive testing (NDT) techniques and passing through measurements of deformation. J Nondestr Eval 2014;33(3): 358–83.
[42] Zhang H, Sfarra S, Saluja K, Peeters J, Fleuret J, Duan Y, Fernandes H, Avdelidis N, Ibarra-Castanedo C, Maldague X. Non-destructive investigation of paintings on canvas by continuous wave terahertz imaging and flash thermography. J Nondestr Eval 2017;36(2):34.
[43] Cennini C. The Craftsman's handbook “il Libro dell'Arte. Dover; 1933.
[44] Blake W. Acrylic painting: a complete guide. Courier Corporation; 1997.
[45] Arora V, Mulaveesala R, Bison P. Effect of spectral reshaping on frequency modulated thermal wave imaging for non-destructive testing and evaluation of steel material. J Nondestr Eval 2016;35(1):1–7.
[46] Ghali VS, Jonnalagadda N, Mulaveesala R. Three-dimensional pulse compression for infrared nondestructive testing. IEEE Sensor J 2009;9(7):832–3.
[47] Gettens RJ, Stout GL. Painting materials : a short encyclopaedia. Dover Publications; 1966.
[48] Carslaw H, Jaeger J. Conduction of heat in solids. second ed. Oxford Clarendon Press; 1959. 1959.
[49] Burgholzer P. Thermodynamic limits of spatial resolution in active thermography. Int J Thermophys 2015;36(9):2328–41.
[50] Lopez F, De Paulo Nicolau V, Ibarra-Castanedo C, Maldague X. Thermal-numerical model and computational simulation of pulsed thermography inspection of carbon fiber-reinforced composites. Int J Therm Sci 2014;86:325–40.
[51] Oelze ML. Bandwidth and resolution enhancement through pulse compression. IEEE Trans Ultrason Ferroelectrics Freq Contr 2007;54(4).
[52] Arora V, Rawat K, Mulaveesala R, Tuli S. Effects of varying bandwidth on frequency modulated thermal wave imaging. J Non-Destr Test Eval 2013;12(2):31–5.
[53] Sekko E, Thomas G, Boukrouche A. A deconvolution technique using optimal Wiener filtering and regularization. Signal Process 1999;72(1):23–32.
[54] Haider B, Lewin PA, Thomenius KE. Pulse elongation and deconvolution filtering for medical ultrasonic imaging. IEEE Trans Ultrason Ferroelectrics Freq Contr 1998; 45(1):98–113.
[55] Gan TH, Pallav P, Hutchins DA. Non-contact ultrasonic quality measurements of food products. J Food Eng 2006;77(2):239–47.
[56] Arora V, Mulaveesala R. Pulse compression with Gaussian weighted chirp modulated excitation for infrared thermal wave imaging. Prog Electromagn Res Lett 2014;44:133–7.
[57] Burrascano P, Laureti S, Ricci M, Senni L, Silipigni G, Tomasello R. Reactance transformation to improve range resolution in pulse-compression detection systems. In: 2017 40th int. Conf. Telecommun. Signal process. IEEE; 2017. p. 480–3.
[58] Pallav P, Gan TH, Hutchins DA. Elliptical-tukey chirp signal for ultrasonic imaging. IEEE Trans Ultrason Ferroelectrics Freq Contr 2007;54(8).
[59] Burrascano P, Callegari S, Montisci A, Ricci M, Versaci M. Ultrasonic nondestructive evaluation systems: industrial application issues. Springer; 2014.
[60] Burrascano P, Laureti S, Senni L, Ricci M. Range sidelobes reduction for pulse-compression NDT based on reactance transformation. In: IEEE international symposium of circuits & systems 2018, Florence 27-30 may; 2018 [Italy (accepted)].
[61] Dua G, Mulaveesala R, Siddique JA. Effect of spectral shaping on defect detection in frequency modulated thermal wave imaging. J Optic 2015;17(2). 025604.
[62] Mulaveesala R, Tuli S. Theory of frequency modulated thermal wave imaging for nondestructive subsurface defect detection. Appl Phys Lett 2006;89(19). 191913.
[63] Laureti S, Silipigni G, Senni L, Tomasello R, Burrascano P, Ricci M. Comparative study between linear and non-linear frequency-modulated pulse-compression thermography. Appl Optic 2018;57(18):D32–9.